Journal of Power Sources 293 (2015) 735–740

Contents lists available at ScienceDirect

Journal of Power Sources

journal homepage: www.elsevier.com/locate/jpowsour

Structural manipulation approaches towards enhanced sodium ionic conductivity in Na-rich antiperovskites

Yonggang Wang [a, b, c], Qingfei Wang [a], Zhenpu Liu [a], Zhengyang Zhou [b], Shuai Li [c], Jinlong Zhu [c], Ruqiang Zou [a, *], Yingxia Wang [b], Jianhua Lin [b], Yusheng Zhao [c, *]

[a] College of Engineering, Peking University, Beijing 100871, China
[b] State Key Laboratory for Rare Earth Materials Chemistry and Applications, College of Chemistry and Molecular Engineering, Peking University, Beijing 100871, China
[c] Department of Physics and Astronomy, University of Nevada, Las Vegas, NV 89154, United States

HIGHLIGHTS

- A series of Na-rich antiperovskites were developed as advanced solid electrolytes.
- The materials are nonflammable, low-cost and suitable for thermoplastic processing.
- Enhanced sodium ionic conductivity was achieved by structural manipulation approaches.
- The Na ionic conductivity of $Na_{2.9}Sr_{0.05}OBr_{0.6}I_{0.4}$ reaches 1.9×10^{-3} S/cm at 200 °C.

GRAPHICAL ABSTRACT

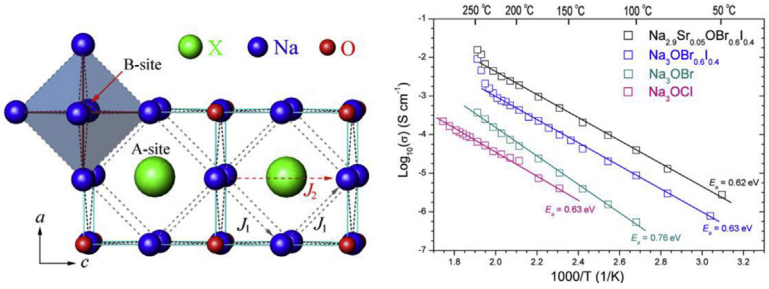

ARTICLE INFO

Article history:
Received 2 April 2015
Received in revised form
29 May 2015
Accepted 1 June 2015
Available online 10 June 2015

Keywords:
Antiperovskite
Solid electrolyte
Sodium ionic conductor
Superionic

ABSTRACT

High-performance solid electrolytes are critical for realizing all-solid-state batteries with enhanced safety and cycling efficiency. However, currently available candidates (sulfides and the NASICON-type ceramics) still suffer from drawbacks such as inflammability, high-cost and unfavorable machinability. Here we present the structural manipulation approaches to improve the sodium ionic conductivity in a series of affordable Na-rich antiperovskites. Experimentally, the whole solid solutions of Na_3OX (X = Cl, Br, I) are synthesized via a facile and timesaving route from the cheapest raw materials (Na, NaOH and NaX). The materials are nonflammable, suitable for thermoplastic processing due to low melting temperatures (<300 °C) without decomposing. Notably, owing to the flexibility of perovskite-type structure, it's feasible to control the local structure features by means of size-mismatch substitution and unequivalent-doping for a favorable sodium ionic diffusion pathway. Enhancement of sodium ionic conductivity by 2 magnitudes is demonstrated by these chemical tuning methods. The optimized sodium ionic conductivity in $Na_{2.9}Sr_{0.05}OBr_{0.6}I_{0.4}$ bulk samples reaches 1.9×10^{-3} S/cm at 200 °C and even higher at elevated temperature. We believe further chemical tuning efforts on Na-rich antiperovskites will promote their performance greatly for practical all-solid state battery applications.

1. Introduction

Lithium-based rechargeable battery is a key technology in our modern life to meet the rapidly increased needs of mobile power

* Corresponding authors.
E-mail addresses: rzou@pku.edu.cn (R. Zou), yusheng.zhao@unlv.edu (Y. Zhao).

http://dx.doi.org/10.1016/j.jpowsour.2015.06.002
0378-7753/

supplies and large-scale energy storage from sustainable sources such as the wind and solar power [1–3]. Besides the well-known technical targets of high energy density and long-cycle lives, advanced rechargeable batteries should also be affordable and exhibit highly enhanced safety [4]. All-solid-state batteries employing inorganic solid electrolytes are the best choice for that they will not suffer from leakage or flammability problems of the currently used liquid or polymeric organic electrolytes [5,6]. However, inorganic materials showing superionic conductivities at ambient or moderate temperatures are rare, most of which are still inflammable chalcogenides [7–10] or oxide ceramics requiring high temperature sintering to reduce the grain-boundary resistance [11,12].

Recently, the observation of superionic conductivity in Li-rich antiperovskites (LiRAP) $Li_3OCl_{1-x}Br_x$ has emblazed a new way to explore advanced solid electrolytes [13]. The idea was inspired from the high temperature superionic conductivity of (K,Na)MgF_3 perovskites by replacing the electronegative anions by electropositive Li^+ [14–17]. The resulting LiRAP materials exhibit low melting points, three-dimensional conducting pathways and high ionic conductivity of $\sigma > 10^{-3}$ S/cm at room temperature. Furthermore, their ionic transport can be readily improved via chemical, electronic and structural manipulation methods and thus serving as high-performance solid electrolytes. In contrast to lithium, the low-cost and earth abundant element sodium is an attractive choice to make large-scale rechargeable batteries especially in the applications of electric vehicles and stationary energy storage in the future [18–21]. When extending the idea of antiperovskites into the rational design of all-solid sodium batteries, we found that there are already several candidates in the inorganic crystal structure database such as Na_3OCl, Na_4OBr_2 and Na_3SO_4F adopting antiperovskite or intergrowth antiperovskite structures [22–24]. Moreover, larger Na^+ (ionic radius 102 pm versus 76 pm of Li^+) is superior to stabilize the antiperovskite structure when take the tolerance factor: $t = (r_A + r_X)/[\sqrt{2}(r_B + r_X)]$ into account, and thus more hidden sodium-based antiperovskite materials are expected [25].

Owing to the high flexibility of a perovskite-type structure, it is easy to perform chemical manipulations such as elemental doping or vacancy generating based on these Na-rich antiperovskite (NaRAP) materials. Here, we can put forward three methods to improve the ionic conductivity of NaRAP electrolytes [13]: 1) A-site mixing with bigger halogen ions; 2) Divalent alkali-earth metal doping in the sodium sites; 3) Depletion to non-stoichiometric. In this work, the results by adopting the former two methods will be presented. We employ the whole solid solutions of Na_3OX (X = Cl, Br, I) to evaluate their potential as solid electrolytes for all-solid sodium battery applications. A facile and timesaving route was developed to obtain the bulky NaRAP samples from the cheapest raw materials of Na, NaOH and NaX. These materials show high sodium-ion conductivity at moderated temperature, which can be further improved by size-mismatch substitution and unequivalent-doping. Our demonstration represents a step further towards the realization of all-solid-state sodium batteries for safe and efficient stationary energy storage.

2. Experimental section

2.1. Syntheses of the NaRAP materials

The solid solutions of Na-rich antiperovskites have been synthesized via a facile solid state reaction under routine pumping. In a typical synthesis of Na_3OCl, 2.00 g NaOH (0.05 mol; analytical reagent (AR), >99% purity) and 2.92 g NaCl (0.05 mol; AR, >99.5% purity) were weighted and ground together in N_2 atmosphere for several minutes. The resulting fine powder was paved on 1.265 g Na metal (0.055 mol; AR, >99.5% purity) and the mixture was placed in a capped alumina crucible and then sealed in a quartz tube. The sample was heated to 150 °C under vacuum at first (past the melting point T_m = 97.8 °C of Na metal) at a heating rate of 1.5 °C/min, then to 350 °C at a heating rate of 10 °C/min. During heating process 1 mol reactant will release 0.5 mol H_2, so that caution and proper disposal must be taken when conduct the experiment and the total amount of the raw materials should be well schemed. After holding at the highest reacting temperature for 3 h, the samples were cooled to room temperature naturally. Phase-pure powders of Na_3OCl could be obtained by repeating the grinding and heating processes for 3 times. The overall synthesis approach of a batch of samples cost about 24 h.

Halogen mixing and divalent alkaline-earth metal doping can be easily achieved via similar method as mentioned above by simply replacing quantitative NaCl with NaX and MX_2 (X = Br, I; M = Mg, Ca, Sr). All the samples were obtained as white, hygroscopic polycrystalline powders, and they were stored in dry inert atmosphere to avoid moisture.

2.2. Characterization

Powder X-ray diffraction (PXRD) data of all the samples were collected at room temperature (25 °C) on a Rigaku D/Max-2000 diffractometer using a rotating anode (Cu Kα, 40 kV and 100 mA), a graphite monochromator and a scintillation detector. Before measurements, the samples were enclosed in a laboratory film (PARAFILM "M") under N_2 atmosphere to avoid moisture absorption. The film contributes to the whole XRD pattern at 21.7°, 24.0° and 74.9° as three small and distinct peaks, which can be easily eliminated in subsequent analyses. The profile-fitting and Reitveld refinements of Na_3OX samples were performed by using program TOPAS 2.1 [26], adopting the previously known cell parameters and atomic positions of Na_3OCl (ICSD-67319) [22] as initial structure model.

Differential thermoanalyses (DTA) analyses were performed using an NETZSCH STA449C instrument in N_2 atmosphere with a heating and cooling rate of 5 °C/min from 50 to 350 °C. For electrochemical impedance measurements, the samples were melted within two gold foils (thickness: 100 μm) at about 280 °C in inert atmosphere, and followed by prolonged annealing at 230 °C to ensure sufficient contacting. The as-obtained pellets had a final diameter of ~7 mm and thickness of about 0.3 mm. AC impedance measurements were then performed using an electrochemical work station analyzer (Zennium, Zahner) at frequencies ranging from 0.1 Hz to 4 MHz and a disturbance voltage of 5 mV. Since the materials are sensitive to moisture and become unstable with oxygen at elevated temperature, all of the measurements were made in dry N_2 atmosphere.

2.3. Sodium migration simulations

The crystal structure of Na_3OCl [22] was employed as the initial structure model to study the sodium migration within the three Na-RAP materials. Cell parameters of Na_3OBr and Na_3OI were used as obtained from the experimental data. The calculations were performed by using CASTEP software [27] (LST/QST) at the GGA level of theory. In each case, a cubic 2 × 2 × 2 supercell of the simple perovskite unit cell containing 40 atoms was used to calculate the sodium migration enthalpy. Sodium vacancies were generated by artificially removing one of the 24 sodium atoms within the supercell. The shortest pathway for sodium ion was generated automatically from one Na site to the nearest vertex of ONa_6 octahedron (vacancy). During the whole calculation process,

the lattice vectors of the supercell were constrained to remain cubic symmetry, but internal ionic relaxations were allowed.

3. Results and discussions

3.1. Syntheses route of NaRAP from sodium metal

Bulk NaRAP powders have been synthesized via a facile and timesaving route from the cheapest raw materials of Na, NaOH and Na*X*. Since the products were sensitive to moisture and would decompose in air atmosphere at high temperature (Figure S1), all the syntheses, material handling processes and measurements were conducted in dry N_2 atmosphere. According to the previous report [13], the isostructural antiperovskites Li_3OX ($X = Cl, Br$) could be fabricated directly from lithium hydroxide and halides by melting them together and pumping out the redundant water. However, our attempts adopting similar methods for Na_3OX failed, probably due to the extraordinary difficulty of NaOH to lose water. Former literature also reported the syntheses of Na_3OCl by employing Na_2O and NaCl to react directly by following equation [22].

$$Na_2O + NaX \rightarrow Na_3OX\ (X = Cl) \quad (1)$$

Nevertheless, commercially available Na_2O reagents are of low purity and are difficult to preserve with the same components. Finally, we decided to use the fresh made "Na_2O" by the following reaction:

$$Na + NaOH \rightarrow Na_2O + 1/2H_2\uparrow \quad (2)$$

And the overall reaction equation is listed as follows:

$$Na + NaOH + NaX \rightarrow Na_3OX + 1/2H_2\uparrow \quad (3)$$

This reaction can be accomplished at relatively low temperature (300–400 °C) and in no more than one day. Experimentally, excess Na metal (5%–10%) was used to eliminate the presence of OH^- in the lattice and therefore its influence on conductivity to the best of our abilities. Fig. 1 shows the powder X-ray diffraction pattern of the as-obtained NaRAP materials. The whole solid solution of $Na_3OCl_{1-x}Br_x$ could be readily obtained with high purity and the main peaks could be indexed in cubic space group *Pm*-3*m* of the antiperovskite structure.

Trace sodium halides (<5% by phase-content analyses, Figure S2) were found as impurity in some of the samples. Pure Na_3OI phase was difficult to achieve in our experiment for that the byproduct Na_4OI_2 emerged as a stable phase in the present reaction condition (Figure S3), which also had an intergrowth RP phase antiperovskite structure. Besides serving as sodium source to provide fresh Na_2O, sodium metal is also an efficient scavenger of the residual hydroxyl in the system. Divalent alkaline-earth metal (Ca^{2+}, Sr^{2+}) doped samples were also synthesized as pure powders via this synthetic route (Figure S4). The new syntheses route is not only high-efficient and timesaving, but also low cost from the cheapest raw materials, making it especially suited to future large-scale production.

3.2. Structure evolution and calorimetry

Structure analyses were performed by using laboratory powder X-ray diffraction technique. The products maintain cubic antiperovskite structure between two end members of Na_3OCl and Na_3OBr, and the cell parameter increases linearly fulfilling the Vegard's law (Figure S5). Based on the high quality PXRD data, we

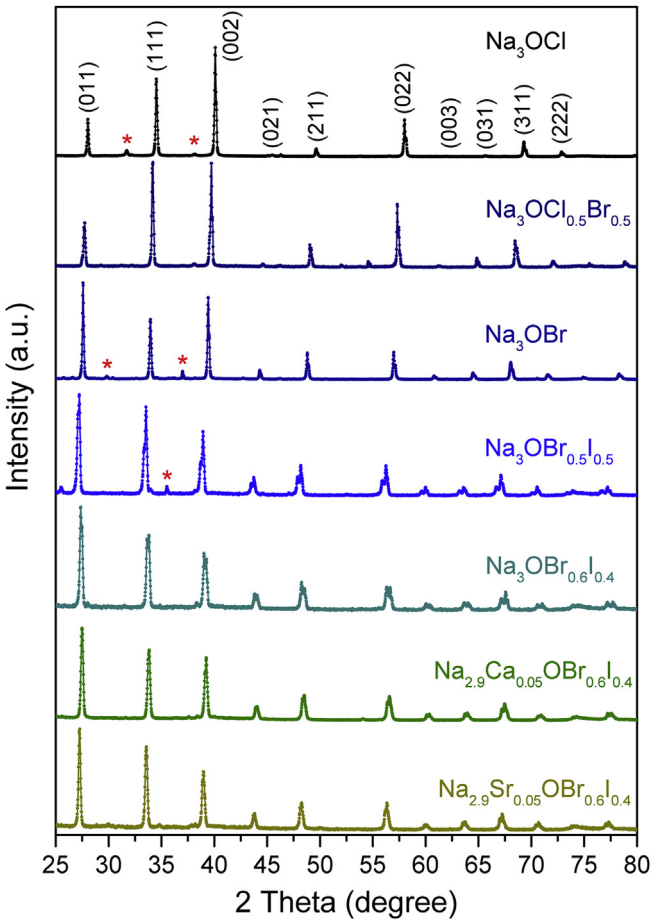

Fig. 1. Powder XRD pattern of antiperovskites Na_3OX (X = Cl, Br, I). The whole solid solutions of $Na_3OCl_{1-x}Br_x$ (x = [0–1]), $Na_3Br_{1-x}I_x$ (x = [0–0.5]) and divalent Ca^{2+}, Sr^{2+} doped samples are obtained as shown from top to bottom. Na_3OCl is indexed in space group *Pm*-3*m*, a = 4.496 Å. Asterisks indicate a small quantity of NaCl or NaBr impurities (<5% mol).

can also give the detailed crystalline data such as atomic positions for Na_3OCl, $Na_3OCl_{0.5}Br_{0.5}$, Na_3OBr, Na_3OI, Na_4OI_2 and $Na_{2.9}Sr_{0.05}OBr_{0.6}I_{0.4}$ by Reitveld refinements (see Table S1–S6). On bigger I^- ion mixing, there was an obvious peak splitting corresponding to possible symmetry breaking down from cubic Na_3OBr to its subgroups for $Na_3OBr_{1-x}I_x$ ($x > 0.1$, Figure S6, S7). Since larger A-site anions will drive the tolerance factor t to a larger value (0.83 for Na_3OCl, 0.87 for Na_3OBr and 0.94 for Na_3OI), the cubic structure of antiperovskite is expected to be stabilized upon I incorporation. Thus, the abnormal symmetry breaking can be attributed to the mismatching effect and possible ordering at the A-sites. Such understanding is supported by the observation that only the peak splitting is observed and no superlattice diffraction appears in the PXRD, whereas the superlattice diffractions are the direct indication for the low symmetry crystalline phases [15,16]. Further experiments for the determination of the exact symmetry and crystal structure are in progress.

Thermal analysis approaches were employed to explore the subtle structural changes of the materials, and the results were shown in Fig. 2. The NaRAPs melted congruently at relative low temperatures, ca. 255 °C for $Na_3OCl_{1-x}Br_x$, and showed tiny divergences between two end members of Na_3OCl, Na_3OBr, and their mixed solid solutions. During cooling, all of the samples showed two distinct exothermic peaks, which might correspond to the possible slow-motion ordering of the halogen ions and subsequent

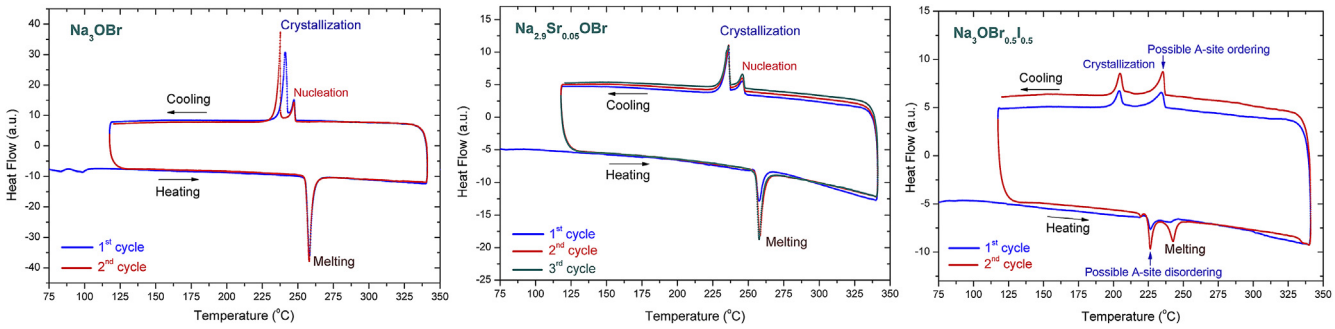

Fig. 2. Differential scanning calorimetry (DSC) curves of the representatives in anti-perovskites Na_3OX (X = Cl, Br, I) solid solution. The observed thermodynamic events (melting, crystallization, possible ordering and phase transition) are marked accordingly.

crystallization to the crystalline state. A small quantity of divalent alkali earth metal doping didn't result in any obvious changes compare to its parent compound. Whereas, I^- ion mixing in the bromine isologues resulted in a notable lowering of melting point to about 240 °C for $Na_3OBr_{0.5}I_{0.5}$, before which a new endothermic peaks located at 226 °C represented possible A-site disordering in the antiperovskite structure. Upon cooling, the temperature interval between "nucleation" and crystallization of $Na_3OBr_{0.5}I_{0.5}$ elongated to about 30 °C, which might be also considered as possible Br^-/I^- ordering within the A-sites. Furthermore, the NaRAP materials could circulate the melting and crystallization processes several times without decomposition, showing their potential facility for hot machining.

3.3. Sodium ionic conductivity

Na and Li-rich antiperovskites that can be served as promising solid electrolytes also benefit from their flexible crystal structures enabling easy chemical manipulations. We noticed two previous reports on the ionic conductivity of antiperovskite Na_3OBr and Na_3OCN gave low values below their melting points [28,29]. In the present work, we demonstrated that both A-site size-mismatch substitution and unequivalent alkali-earth-metal doping could improve the ionic conducting performance remarkably. Fig. 3 shows the representative conductivity measurement results for the halogen-mixed and alkali-earth metal doped Na_3OX solid solutions at moderate temperatures. Most of the impedance plots consist of a semicircle and a spike, respectively corresponding to contributions from the grain of the crystalline electrolyte and an inter-electrode capacitance. These typical Nyquist plots clearly indicate pure ionic conductive characteristics of the present antiperovskite materials. While in very a few cases when the pellets are not well-distributed, the contributions from both bulk grain and grain boundary can be observed (Figure S8). The derived ionic conductivities for $Na_3OBr_{0.6}I_{0.4}$ are 9.80×10^{-5} S/cm at 160 °C, 2.26×10^{-4} S/cm at 180 °C, and 4.30×10^{-4} S/cm at 200 °C. When a spot of divalent Sr^{2+} ions were doped into the Na sites (Na^+ vacancies introduced by the defect chemistry: $Na_{2.9}\square_{0.05}Sr_{0.05}OBr_{0.6}I_{0.4}$), the value can boost to 2.06×10^{-4} S/cm at 140 °C, and 9.50×10^{-4} S/cm at 180 °C. The activation energies for ionic conduction calculated based on the equation: $\sigma T = A_0 \times \exp(-E_a/kT)$ are 0.76 eV for Na_3OBr, 0.63 eV for $Na_3OBr_{0.6}I_{0.4}$ and 0.62 eV for $Na_{2.9}Sr_{0.05}OBr_{0.6}I_{0.4}$, respectively. They are comparable with other typical sodium superionic conductors such as Na_3PS_4 and $Na_3ZrSi_2PO_{12}$ [9,11], but much higher than those of Li-rich antiperovskite superionic conductors (~0.23 eV), which is reasonable considering the larger ionic radius of Na^+ than Li^+.

Fig. 4 shows the Arrhenius plots of several representatives of the

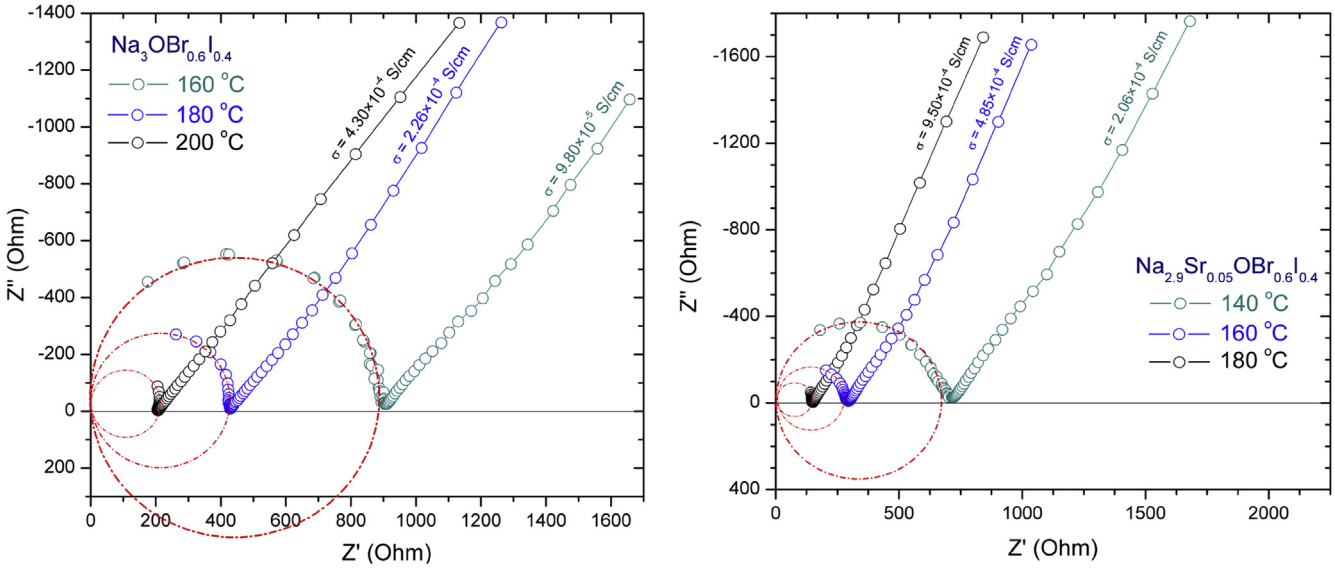

Fig. 3. Impedance spectroscopy Nyquist plots of the real and imaginary components of the halogen-mixed $Na_3OBr_{0.6}I_{0.4}$ and Sr-doped $Na_{2.9}Sr_{0.05}OBr_{0.6}I_{0.4}$ measured at different temperatures.

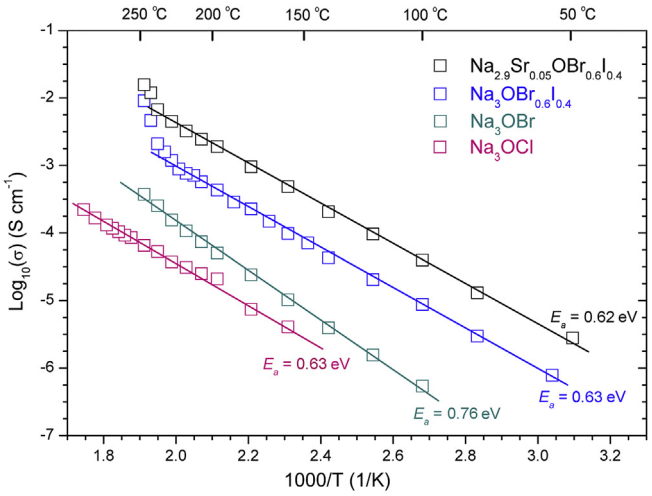

Fig. 4. Arrhenius plots of log(σ) versus 1/T for pure Na_3OCl, Na_3OBr, halogen-mixed $Na_3OBr_{0.6}I_{0.4}$ and alkali-earth ion doped $Na_{2.9}Sr_{0.05}OBr_{0.6}I_{0.4}$ antiperovskites. The activation energies E_a are derived by the slopes of the linear fitting of $\ln(\sigma T) = -E_a/kT$.

NaRAP materials. The sodium ionic conductivities step up from pure Na_3OCl to Na_3OBr and then to iodine-mixed $Na_3OBr_{0.6}I_{0.4}$, which may be attributed to the mismatching effect by the incorporation of bigger halogen ions in the A-sites. Alternate Br and I anions with diverse ionic radii in the dodecahedral A-sites within the three-dimensional lattice will provide much free space for the Na^+ ions to hop in and pass through, via interstitial route, *i.e.* Frenkel style. On the other hand, divalent Sr^{2+} doping in the Na^+ sites will consequentially introduce more vacancies, which are essential to provide effectual diffusion pathway for high ionic conductivity, *i.e.* Schottky style. Detailed data of the sodium ionic conductivity of $Na_3OCl_{1-x}Br_x$ (x = 0, 0.2, 0.5, 0.8, 1) and $Na_{2.9}M_{0.05}OBr_{0.6}I_{0.4}$ (M = Ca, Sr) are provided in Figure S9. The optimized conductivity of $Na_{2.9}Sr_{0.05}OBr_{0.6}I_{0.4}$ is more than two magnitudes higher than that of pure Na_3OBr, and reaches 2.78×10^{-6} S/cm at room-temperature, 1.89×10^{-3} S/cm at 200 °C, and even beyond 10^{-2} S/cm when temperature approaches the melting point. These results show great potential of NaRAP materials as advanced electrolytes in the applications of advanced all-solid-state sodium batteries that operated at moderated temperatures (such as the stationary energy storage).

Fig. 5 shows the crystal structure of antiperovskite Na_3OX (X = Cl, Br, I) with cubic symmetry and space group Pm-3m. In analogy to the perovskite structure, ONa_6 octahedra share their corners with each other to form a three dimensional framework and the halogen anions occupy the 12-coordinated A-sites. We highlight the two possible diffusion pathways for Na^+ ions along [101] and [001] directions when takes a certain vacancy concentration into account. To gain insight into the chemical manipulations towards advanced ionic conductivity, we perform a primary DFT simulation to evaluate the effect of different A-site ionic radius on sodium ion migrations within the NaRAP materials. Fig. 6 shows the calculated sodium migration barrier from one Na site to the nearest vertex of ONa_6 octahedron (vacancy): 0.428 eV for Na_3OCl, 0.315 eV for Na_3OBr and 0.311 eV for Na_3OI, respectively. These values are a little smaller than the measured active energies but reasonable considering the neglect of the vacancy formation energy when perform theoretical calculation. Significantly, the results evidently support the idea that larger A-site anions are favorable for the migration of sodium ions contrast to that of lithium ions within the same antiperovskite structure. Future research efforts considering larger anion groups such as BF_4^-, BH_4^- as the A-site components would be highly recommended.

It is also known that there are many other complications that will significantly influence the bulk conductivity of the antiperovskites, such as the local disorder, microstructure, and even thermal treatment history [13]. As a proof-of-concept experiment, we only conduct chemical mixing and doping approaches on the simplest cubic antiperovskites Na_3OX to illustrate the distinct promotion of ionic conductivity. Considering the all above-mentioned facts, we may foresee that there is still much room in the improvements and explorations of novel Na-rich antiperovskites as advanced solid electrolytes for next-generation sodium batteries. Future investigations should pay special attentions to the refined crystal structure, optimization of the preparation conditions, and discovery of more Na-rich compounds with antiperovskite or their intergrowth structures.

4. Conclusions

In summary, we demonstrate great improvement of the sodium ionic conductivity in Na-rich antiperovskites by chemical manipulation approaches. A facile and timesaving route was established to fabricate the whole solid solutions of Na_3OX (X = Cl, Br, I). Structural, calorimetric and electrochemical analyses were employed to evaluate the sodium ionic conductivity performance of these materials. Primary results show that the NaRAP materials exhibit high sodium ionic conductivity at moderated temperatures (>10^{-3} S/cm at about 200 °C), promising to be applied for advanced all-solid-state sodium batteries. More importantly, halogen-size-mismatch substitution and nonequivalent-doping of sodium ions by alkali-earth ions can remarkably promote the sodium

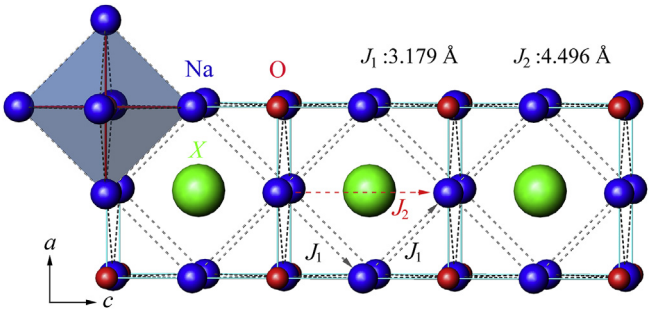

Fig. 5. Representation of the crystal structure of the antiperovskites Na_3OX (X = Cl, Br, I). ONa_6 octahedron is shown in blue and dashed lines show the nearest Na–Na distances and J_1, J_2 indicate the two possible diffusion pathways of Na^+ ions within the lattice. (For interpretation of the references to colour in this figure legend, the reader is referred to the web version of this article.)

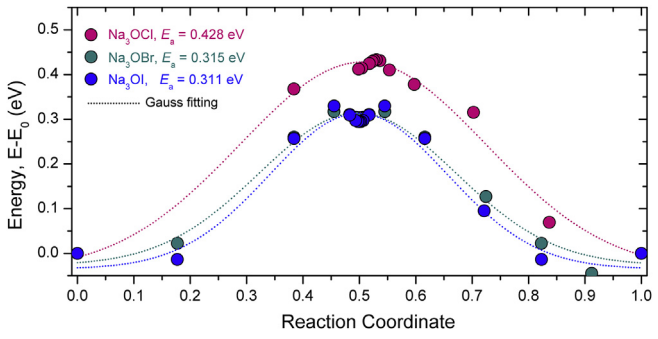

Fig. 6. Energy for sodium migration in NaRAP. The end members of Na_3OX (X = Cl, Br, I) are compared and the sodium migration is considered along the minimum energy pathway (J_1 as indicated in Fig. 5).

conductivity of the novel NaRAP materials, which endows expansive room for further investigations. Since sodium is cheap and abundant in the world, and there are obviously many already known and undiscovered Na-rich compounds adopting anti-perovskite or their derived structures [23], the development of low-cost rechargeable sodium batteries using NaRAP materials will greatly promise the realization of high-efficiency mobile power supply and large-scale energy storage.

Acknowledgment

We greatly appreciate the funding support by the National Natural Science Foundation of China 51322205 and 21371014, New Star Program of Beijing Committee of Science and Technology (2012004), and the Ministry of education program for New Century Excellent Talents of China (NCET-11-0027). We thankfully acknowledge Prof. Z. S. Lin (TIPC, CAS) and Z. L. Lang for experimental assistance and discussions in theoretical calculations using CASTEP. We also acknowledge Prof. D. G. Xia (PKU) for useful discussions.

Appendix A. Supplementary data

Supplementary data related to this article can be found at http://dx.doi.org/10.1016/j.jpowsour.2015.06.002.

References

[1] M. Armand, J.-M. Tarascon, Nature 451 (2008) 652–657.
[2] J.B. Goodenough, K.S. Park, J. Am. Chem. Soc. 135 (2013) 1167–1176.
[3] R. Marom, S.F. Amalraj, N. Leifer, D. Jacob, D. Aurbach, J. Mater. Chem. 21 (2011) 9938–9954.
[4] F. Cheng, J. Liang, Z. Tao, J. Chen, Adv. Mater. 23 (2011) 1695–1715.
[5] P. Knauth, Solid State Ionics 180 (2009) 911–916.
[6] J.-M. Tarascon, M. Armand, Nature 414 (2001) 359–367.
[7] H. Yamane, M. Shibata, Y. Shimane, T. Junke, Y. Seino, S. Adams, K. Minami, A. Hayashi, M. Tatsumisago, Solid State Ionics 178 (2007) 1163–1167.
[8] N. Kamaya, K. Homma, Y. Yamakawa, M. Hirayama, R. Kanno, M. Yonemura, T. Kamiyama, Y. Kato, S. Hama, K. Kawamoto, A. Mitsui, Nat. Mater. 10 (2011) 682–686.
[9] A. Hayashi, K. Noi, A. Sakuda, M. Tatsumisago, Nat. Commun. 3 (2012) 856.
[10] Z. Liu, W. Fu, E.A. Payzant, X. Yu, Z. Wu, N.J. Dudney, J. Kiggans, K. Hong, A.J. Rondinone, C. Liang, J. Am. Chem. Soc. 135 (2013) 975–978.
[11] O. Bohnke, S. Ronchetti, D. Mazza, Solid State Ionics 122 (1999) 127–136.
[12] S. Lupart, G. Gregori, J. Maier, W. Schnick, J. Am. Chem. Soc. 134 (2012) 10132–10137.
[13] Y. Zhao, L.L. Daemen, J. Am. Chem. Soc. 134 (2012) 15042–15047.
[14] M. O'keeffe, J.-O. Bovi, Science 206 (1979) 599–600.
[15] Y. Zhao, D.J. Weidner, J.C. Parise, D. Cox, Phys. Earth Planet. Inter. 76 (1993) 1–34.
[16] Y. Zhao, J. Solid State Chem. 141 (1998) 121–132.
[17] A. Yoshiasa, D. Sakamoto, H. Okudera, M. Sugahara, K. Ota, A. Nakatsuka, Z. Anorg. Allg. Chem. 631 (2005) 502–506.
[18] N. Yabuuchi, M. Kajiyama, J. Iwatate, H. Nishikawa, S. Hitomi, R. Okuyama, R. Usui, Y. Yamada, S. Komaba, Nat. Mater. 11 (2012) 512–517.
[19] P. Hartmann, C.L. Bender, M. Vračar, A.K. Dürr, A. Garsuch, J. Janek, P. Adelhelm, Nat. Mater. 12 (2013) 228–232.
[20] J. Song, Z. Yu, M.L. Gordin, S. Hu, R. Yi, D. Tang, T. Walter, M. Regula, D. Choi, X. Li, A. Manivannan, D. Wang, Nano Lett. 14 (11) (2014) 6329–6335.
[21] Z. Yu, J. Song, M.L. Gordin, R. Yi, D. Tang, D. Wang, Adv. Sci. 2 (2015) 1400020.
[22] K. Hippler, S. Sitta, P. Vogt, H. Sabrowsky, Acta Cryst. C46 (1990) 736–738.
[23] H. Sabrowsky, K. Hippler, S. Sitta, P. Vogt, Acta Cryst. C46 (1990) 368–369.
[24] L. Fanfani, G. Fiuseppetti, C. Tadini, P.F. Zanazzi, Mineral. Mag. 43 (1980) 753–759.
[25] S.V. Krivovichev, Z. Krist. 223 (2008) 109–113.
[26] Topas V2.1, General Profile and Structure Analysis Software for Powder Diffraction Data, Bruker AXS, Karlsruhe, Germany, 2002.
[27] S.J. Clark, M.D. Segall, C.J. Pickard, P.J. Hasnip, M.J. Probert, K. Refson, M.C. Payne, Z. Krist. 220 (2005) 567.
[28] W. Müller, M. Jansen, Z. Anorg. Allg. Chem. 591 (1990) 41–46.
[29] M. Jansen, C. Feldmann, W. Müller, Z. Anorg. Allg. Chem. 611 (1992) 7–10.